Journal of Molecular Graphics and Modelling 72 (2017) 58–69

Contents lists available at ScienceDirect

Journal of Molecular Graphics and Modelling

journal homepage: www.elsevier.com/locate/JMGM

First principles study for the key electronic, optical and nonlinear optical properties of novel donor-acceptor chalcones

Shabbir Muhammad[a,b,c,*], Abdullah G. Al-Sehemi[c,d], Zhongmin Su[a], Hongliang Xu[a,*], Ahmad Irfan[c,d], Aijaz Rasool Chaudhry[b,c]

[a] Institute of Functional Materials Chemistry, Faculty of Chemistry, Northeast Normal University, Changchun 130024, Jilin, People's Republic of China
[b] Department of Physics, Faculty of Science, King Khalid University, Abha 61413, P.O. Box 9004, Saudi Arabia
[c] Research Center for Advanced Materials Science (RCAMS), King Khalid University, Abha 61413, P.O. Box 9004, Saudi Arabia
[d] Department of Chemistry, Faculty of Science, King Khalid University, Abha 61413, P.O. Box 9004, Saudi Arabia

ARTICLE INFO

Article history:
Received 24 October 2016
Received in revised form
10 December 2016
Accepted 12 December 2016
Available online 14 December 2016

Keywords:
Nonlinear optical properties
Chalcones
Second hyperpolarizability
Density of states
Second hyperpolarizability density analysis

ABSTRACT

Using first-principle methods, several key electronic, optical and nonlinear optical properties are calculated for two recently synthesized chalcone derivatives i.e. (2E)-3-(4-methylphenyl)-1-(3-nitrophenyl)prop-2-en-1-one (comp.**1**) and (2E)-3-[4-(dimethylamino)phenyl]-1-(3-nitrophenyl)prop-2-en-1-one (comp.**2**). The calculation of dipole moment, polarizability <α>, anisotropy of polarizability as well as second hyperpolarizability (usually considered as a signature for two photon absorption phenomenon) are performed using density functional theory methods at PBE0/6-311G** level of theory. The linear average polarizability <α> for comp.**1** and comp.**2** are found to be 32.15×10^{-24} and 38.76×10^{-24} esu, respectively. Similarly, the second hyperpolarizability <γ> amplitudes of comp.**1** and comp.**2** are found to be reasonably larger mounting to 79.31×10^{-36} and 181.36×10^{-36} esu, respectively. The importance of donor end is determined by comparing *p*-methylphenyl group of comp.**1** with that of *N*,*N*-dimethylaniline group of comp.**2** that results a remarkable increase in its <γ> amplitude, which is ~2 times larger as compared with that of comp.**1** owing to the stronger donor-acceptor configuration of comp.**2**. Interestingly, a comparison of average static third-order nonlinear polarizabilities <γ> shows that <γ> amplitudes of comp.**1** and comp.**2** are ~13 times and ~29 times larger than that of *para*-nitroaniline (a typical standard push-pull NLO-phore) at the same PBE0/6-311G** level of theory, which indicates a real time NLO application of our titled compounds. Time dependent density functional theory (TD-DFT) calculations along with frontier molecular orbitals, density of states (DOS), second hyperpolarizability density analysis and molecular electrostatic potential (MEP) diagrams are used to trace the origin of electro-optical as well as structure property relationships.

© 2016 Elsevier Inc. All rights reserved.

1. Introduction

The structure of any material strongly determines the interaction of light photons passing through it. The optical materials are very crucial to compose the key components for optical systems and laser applications, which is perhaps the major field of scientific study in present era [1,2]. Since the discovery of first function laser, there has been significant scientific interest in the field of nonlinear optical (NLO) materials. The NLO material has the ability to change the frequency of incident laser by interacting with it. There has been realized several application of NLO materials in modern hi-tech era. The NLO materials generate new electromagnetic fields having different phases and frequencies by interacting with intense laser light, which leads to its novel applications in frequency doubling and mixing, holographic imaging, optical data storage, and telecommunication etc [3]. In the past, several design rules were used to guide synthetic explorations NLO materials. In addition to these rules, the synthetic chemistry of present era has used the intuitive of reliable computational techniques to synthesize many interesting NLO-phores [4]. Over the few decades, a verity of materials has been explored for NLO applications. Broadly speaking, these include organic, inorganic, organometallic and organic-inorganic hybrid materials [5–8]. Recently several theoretical and experimental studies have been

* Corresponding authors at: Institute of Functional Materials Chemistry, Faculty of Chemistry, Northeast Normal University, Changchun 130024, Jilin, People's Republic of China.
E-mail addresses: mshabbir@kku.edu.sa (S. Muhammad), hlxu@nenu.edu.cn (H. Xu).

http://dx.doi.org/10.1016/j.jmgm.2016.12.009
1093-3263/© 2016 Elsevier Inc. All rights reserved.

devoted to organic NLO-phores because of their easy in fabrication, diverse variety of structures and relatively low economical cost [9]. Among the organic molecules, chalcones are the front running candidates that have been significantly synthesized and tested for their NLO applications. For instance, the single crystal of 3,4-dimethoxy chalcone were grown and investigated of their electro-optical properties by Sajan et al. [10]. The role of pyridine ring to modulate NLO properties of pyridine based chalcone single crystals have been checked by Menezes et al. [11]. Similarly, the computationally calculated static first hyperpolarizabity has been used, in addition to synthesis and characterization of 1,5-di-*p*-tolylpenta-1,4-dien-3-one (DTDO) by Prasad et al. [12]. Additional noticeable chalcone syntheses and characterizations include 2*E*)-3-(2-methylphenyl)-1-(4-nitrophenyl) prop-2-en-1-one [13], 1-(3-Nitrophenyl)-5-phenylpenta-2,4-dien-1-one [14], 2-cyano-*N*-(1-phenylethyl) acetamide [15] 3-(3-fluorophenyl)-1-[4-(methylsulfanyl) phenyl] prop-2-en-1-one [16], and 1-(4-Bromophenyl)-3-(napthalen-2-yl)prop-2-en-1-one ($C_{19}H_{13}BrO$) [17] etc. The above reported chalcone derivatives have been characterized and also checked for the NLO efficiency. Recently, we have also highlighted many strategies to finely tune the NLO properties of many different types of compounds including lithiation effect [18], proton abstraction [19], bridging core modification [20] and tuning of push-pull configurations [21,22] etc. Nevertheless, recent studies highlight the potential of donor-acceptor chalcones as potential candidate for efficient NLO materials. The motivation of present study is to use modern quantum chemical methods to highlight some recently reported single crystals of donor-acceptor chalcone derivatives consisting of (2E)-3-(4-methylphenyl)-1-(3-nitrophen-yl)prop-2-en-1-one [23] (hereafter refer as comp.**1**) and (2E)-3-[4-(dimethylamino)phenyl]-1-(3-nitrophenyl)prop-2-en-1-one [24] (hereafter refer as comp.**2**). To the best of our knowledge, there is no study on the above reported compounds regarding their optical and nonlinear optical properties. Unlike the several above reported chalcones, the compounds in present investigation possess donor-acceptor configurations, which are rare and vital to make them promising for NLO applications. Interestingly, among the huge pile of publications regarding NLO properties, a few deal with third-order NLO properties as in present investigation. Moreover, the impact of only tuning the strength of donor in donor-acceptor configuration will also be investigated by comparing the optical and nonlinear optical properties of these closely related compounds, which possess different donor moieties i.e. (comp.**1** having 4-methylphenyl and comp.**2** containing 4-dimethylaminophenyl). Thus the present investigation will not only highlight the potential of selected compounds as efficient third-order NLO-phores but also features a comparative analysis to modulate such compounds for their potential use in optical and nonlinear optical devices etc.

2. Computational details

All calculations for molecular level study have been performed using Gaussian suit of programs [25] in present investigation. The isolated molecular geometries have been fully optimized without ant symmetry constrains at PBE0/6-311G** level of theory. The subsequent frequency calculations have been also performed to confirm the optimized structures as global minima on potential energy surface. For a molecule, it is not always true that a method reproducing geometrical parameters accurately can also predict correctly its NLO properties. In this regard, we have guessed the performance of different functionals including B3LYP, PBE0, M06 Cam-B3LYP and HF to calculated dipole moments, polarizability and second hyperpolarizability using 6-311G** basis set. The results are presented in the form of graphical comparisons as shown in Fig. 1. From Fig. 1, it can be seen that for compounds **1** and **2**, their amplitudes of dipole moments, polarizability and static second hyperpolarizability γ are the largest and the smallest with B3LYP and HF functionals, respectively. While on the other hand, PBE0, M06 and Cam-B3LYP provide results that are reasonably agree with each other as seen in Fig. 1(a), (b) and (c), respectively. Similarly, a linear fitting of these curves indicates that all three properties calculated with PBE0 provide well agreement with all other methods. Additionally, several previous investigations showed that PBE0 could outperform than the other global hybrids yielding reasonable simulations for many chemophysical properties especially providing theoretically correct description of ground and excited states [26,27]. Based on the above results of our test calculations, comparison of geometrical parameters, and several previous studies, we chose PBE0 functional for further all calculations in present investigation. The calculations for dipole moment, polarizability and second hyperpolarizability are performed using the PBE0 method with 6-311G** basis set. The TD-PBE0 has been used to calculate the absorption and emission spectra of the comp.**1** and **2**. A well-known finite field (FF) method is used to calculate the polarizability and second hyperpolarizability. Originally, Kurtz et al. [28] have developed the FF method, which is subsequently used not only by theoretician but also many experimentalists to assess the NLO properties of several types of materials [29]. The FF method has provided very consistent results with experiments as well as with other theoretical approaches like response theory and Time-dependent-sum over states (TD-SOS) methods for studying the structure-NLO property relationships in many investigations [30]. A static electric field (F) is applied in FF approach and the energy (E) of the molecule is given by following Eq.

$$E = E^{(0)} - \mu_1 F_1 - \frac{1}{2}\alpha_{ij}F_iF_j - \frac{1}{6}\beta_{ijk}F_iF_jF_k - \frac{1}{24}\gamma_{ijkl}F_iF_jF_kF_l - \dots \quad (1)$$

In the absence of an electronic field, the total energy of molecule is represented by $E^{(0)}$ μ is the dipole moment, α is the polarizability, β and γ are the first and second hyperpolarizabilities, respectively, while x, y *and* z label the i, j *and* k components, respectively. It can be seen from above equation that differentiating E with respect to F obtains the μ, α, β, and γ values. Here β, and γ values represent the origin of second-order (χ^2) and third-order (χ^3) nonlinear optical (NLO) susceptibilities, respectively.

The electronic dipole moment, linear polarizability, anisotropy of polarizability and second hyperpolarizability are calculated using following relations as defined under:

$$\mu = \left(\mu_x^2 + \mu_y^2 + \mu_z^2\right) \quad (2)$$

The average polarizability (α_0) can be calculated by following equations:

$$\alpha_0 = \frac{1}{3}\left(\alpha_{xx} + \alpha_{yy} + \alpha_{zz}\right) \quad (3)$$

For anisotropy of polarizability ($\Delta\alpha$) that implies the dependence of the potential energy on the orientation of electronic cloud with respect to the collision (body-fixed) axis and it can be calculated by following Equation,

$$\Delta\alpha = \frac{1}{\sqrt{2}}\sqrt{\left[(\alpha_{xx} - \alpha_{yy})^2 + (\alpha_{yy} - \alpha_{zz})^2 + (\alpha_{zz} - \alpha_{xx})^2 + 6\alpha_{xz}^2\right]} \quad (4)$$

$$\langle\gamma\rangle = \frac{1}{15}\sum_{ij=x,y,z}\left(\gamma_{iijj} + \gamma_{ijij} + \gamma_{ijji}\right). \quad (5)$$

Assuming Kleinmann symmetry, these are reduced to six components at least for static second hyperpolarizability.

$$\langle\gamma\rangle = \frac{1}{5}\left(\gamma_{xxxx} + \gamma_{yyyy} + \gamma_{zzzz} + 2\left(\gamma_{xxyy} + \gamma_{xxzz} + \gamma_{yyzz}\right)\right). \quad (6)$$

Table 1
The dipole moments (a. u.)[a] of comp.**1** and comp.**2** in ground and excited states as calculated at PBE0 and TD-PBE0 methods, respectively.

Comp.**1**			Comp.**2**		
Dipole moment	Ground State	Excited State	Dipole moment	Ground State	Excited State
μ_x	−0.08	−0.01	μ_x	−0.12	0.12
μ_y	1.83	1.87	μ_y	1.95	1.30
μ_z	2.68	5.71	μ_z	4.20	15.92
μ_{tot}	3.25	6.01	μ_{tot}	4.63	15.98

[a] 1 a. u. of electric dipole moment = 2.541 Debye = 2.541×10^{-18} esu-cm.

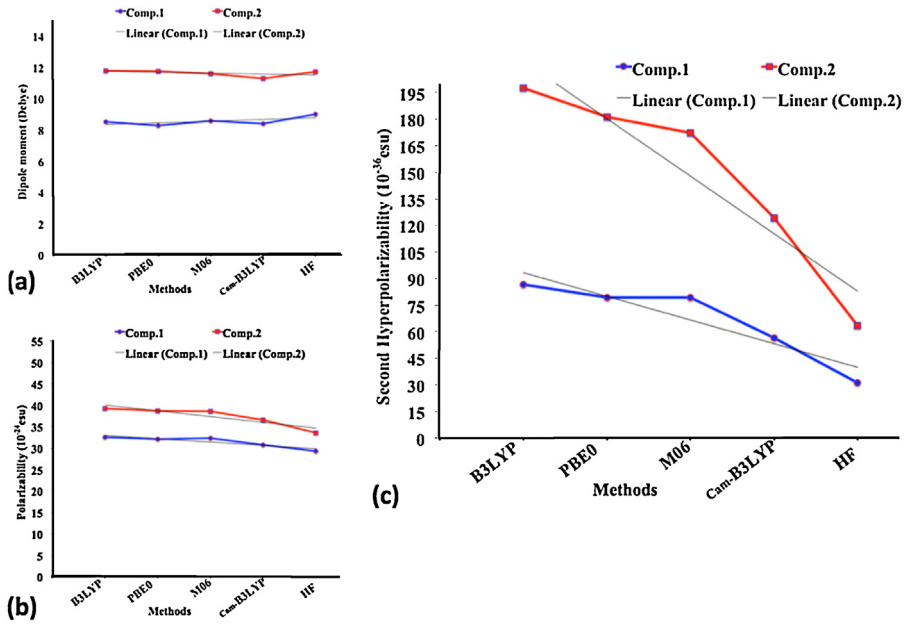

Fig. 1. The graphical comparison of dipole moments, polarizability and third-order nonlinear polarizability at different methods where straight lines indicates the linear fitting of curves.

The components of γ amplitude in terms of Cartesian coordinates have been calculated using GAUSSIAN 09.

3. Results and discussion

3.1. Molecular geometries

The molecular structures of selected comp.**1** (2E)-3-(4-methylphenyl)-1-(3-nitrophen-yl)prop-2-en-1-one and comp.**2** (2E)-3-[4-(dimethylamino)phenyl]- 1-(3-nitrophenyl)prop-2-en-1-one are shown in Fig. 2 along with indication of their important geometrical parameters. The difference between geometries of above titled compounds is only at the donor end, which is 4-methylphenyl and 4-(dimethylamino)phenyl groups for comp.**1** and comp.**2**, respectively (see Fig. 2). As their single crystal geometries are already reported, we have extensively compared the optimized geometries with their experimental single crystal structures as given in S1. A graphical representation about the comparison of optimized bond lengths in gas phase, with periodic boundary conditions (PBC) as well as with experimentally reported crystal structure has been shown in Fig. 3. It is important to mention that the experimental crystallographic structures are reported in solid so we also used periodic boundary conditions to separately optimize the structures and to check the solid-state effects. From Fig. 3, it can be seen that there is reasonably good agreement among the bond lengths as compared among experimentally reported crystallographic, calculated in gas phase and with periodic boundary conditions for comp.**1** and comp.**2**. A somewhat similar trend is also found in bond angles and torsion angles as compared in gas phase geometries with experimental and with periodic boundary conditions for comp.**1** and comp.**2** (see Table S1 of Supporting information). Thus a reasonable agreement among calculated and experimental geometrical parameters as well as a good agreement among different computational methods is encouraging the use of selected methodology (PBE0/6-311G**) in present investigation.

3.2. Dipole moment and polarizability

The calculated dipole moments for comp.**1** and comp.**2** in their ground and excited states have been shown in Table 1. In ground state the dipole moments of comp.**1** and comp.**2** are found to be 3.25 a. u. (8.257 D) and 4.63 a. u. (11.769 D), respectively. A careful analysis of individual components shows that the major dipole moment components are in *yz*-plane as indicated by dominant components of μ_z and μ_y in Table 1. This is because the charge transfer axis is mainly aligned with *yz*-plane while *x*-axis is negligible being out of plane. In its ground and excited states, the larger dipole moment value of comp.**2** can be attributed to its stronger donor-acceptor configuration as compared with those of comp.**1**. There are also significant increments from ground to excited states dipole moments, which are 6.01 a. u. and 15.98 a. u., for comp.**1** and comp.**2**, respectively. The significant enhancement of excited state dipole moments are due to the intramolecular charge transfer between donor and acceptor moieties of these compounds, which is larger in case of comp.**2** probably owing to it stronger donor-acceptor configuration.

Furthermore, for comp.**1** and comp.**2**, their calculated linear polarizabilities (α_0) along with their individual components are

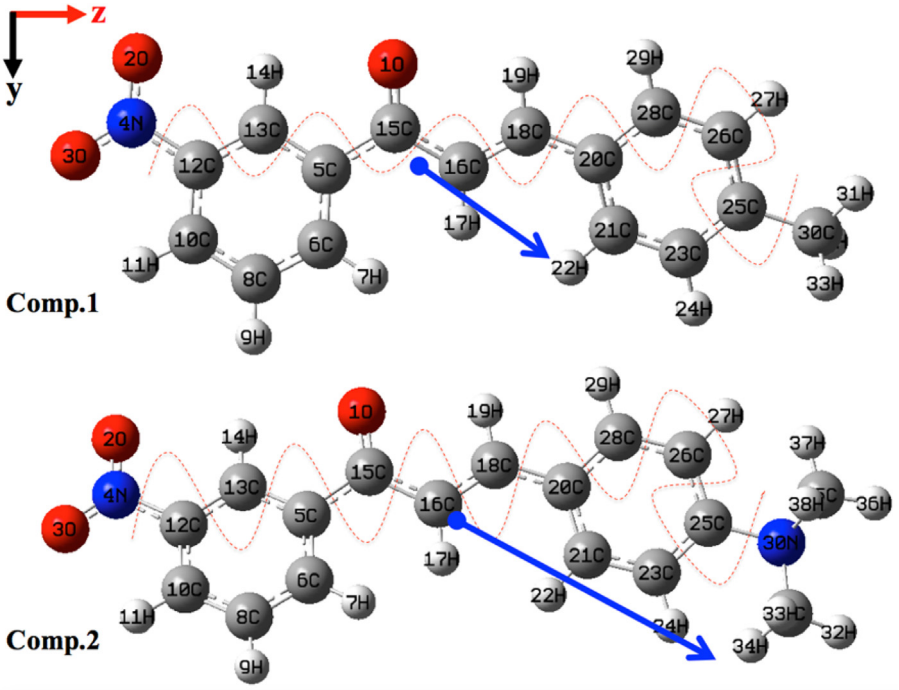

Fig. 2. The optimized geometries of comp.**1** and comp.**2** at PBE0/6-311G** level of theory. The blue arrows indicate the directions of dipole moments and dotted redlines circumvallate the most important geometrical parameters as compared with experimental crystal data in present investigation. (For interpretation of the references to colour in this figure legend, the reader is referred to the web version of this article.)

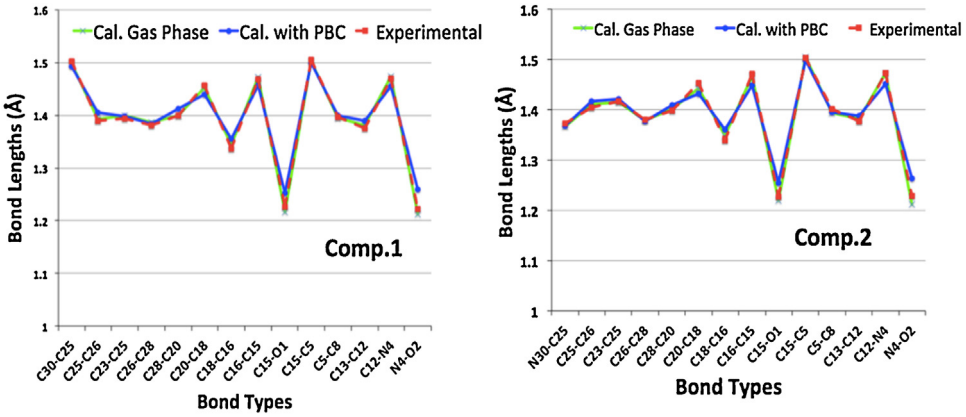

Fig. 3. The graphical representation of the comparison of bond lengths as determined in gas phase, periodic boundary condition and in experimental structure.

Table 2
The average polarizability, its individual components and anisotropic polarizability as calculated at PBE0/6-311G** level of theory.

Comp.**1**			Comp.**2**		
α Components	a. u.	$\times 10^{-24}$ esu	α Components	a. u.	10^{-24} esu
α_{xx}	83	12.30	α_{xx}	97	14.42
α_{xy}	10	1.48	α_{xy}	−8	−1.25
α_{yy}	252	37.34	α_{yy}	256	37.96
α_{xz}	1	0.22	α_{xz}	−1	−0.22
α_{yz}	86	12.71	α_{yz}	−99	−14.69
α_{zz}	316	46.81	α_{zz}	431	63.90
<α>	217	32.15	<α>	262	38.76
α_{aniso}	256	37.98	α_{aniso}	336	49.79

also collected in Table 2. It is important to mention here that linear polarizabilities and third-order nonlinear polarizabilities are calculated in dipole orientation i.e. aligning *z*-axis along the direction of dipole moments. This is because of experimental procedures that usually calculate the polarizabilities along the dipole orientations. From Table 2, it can be seen that the linear average polarizability <α> for comp.**1** and comp.**2** are 32.15×10^{-24} and 38.76×10^{-24} esu, respectively. A careful analysis of individual components shows that their components (α_{zz}) along the dipole orientations show the largest polarizability values of 46.81×10^{-24} and 63.90×10^{-24} esu for comp.**1** and comp.**2**, respectively, as compared to their other individual components as well as to those of their average polarizabilities. The dependence of polarizability on the direction of electric field is also noticeable in terms of its larger isotropic polarizability values, which are 37.98×10^{-24} and 49.79×10^{-24} esu for comp.**1** and comp.**2**, respectively.

3.3. Third-order nonlinear polarizability (γ)

In addition to their polarizabilities, we have also calculated the third-order nonlinear polarizabilities (γ) of comp.**1** and comp.**2** at the same PBE0/6-311G** level of theory. As compounds **1** and

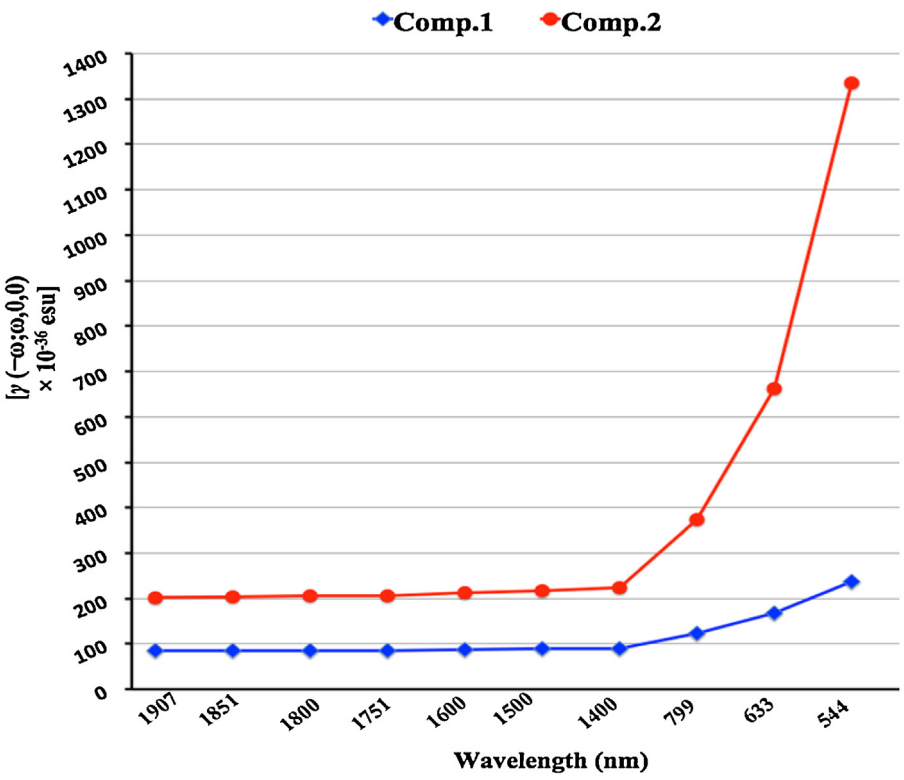

Fig. 4. The plot of frequency dependent γ amplitudes $\gamma(-\omega;\omega,0,0)$ at various wavelengths of incident laser.

Table 3
The average third-order nonlinear polarizabilities <γ> along with their individual components for comp.**1** and comp.**2** at PBE0/6-311G** level of theory.

Comp.**1**			Comp.**2**		
γ	$\times 10^3$ a. u.	$\times 10^{-36}$ esu	**γ**	$\times 10^3$ a. u.	$\times 10^{-36}$ esu
γ_{xxxx}	1.189	0.60	γ_{xxxx}	3.00	1.55
γ_{yyyy}	96.225	48.47	γ_{yyyy}	85.00	42.93
γ_{zzzz}	401.535	202.26	γ_{zzzz}	1234	621.44
γ_{xxyy}	1.529	0.77	γ_{xxyy}	4.00	1.87
γ_{xxzz}	2.124	1.07	γ_{xxzz}	4.00	2.08
γ_{yyzz}	140.515	70.78	γ_{yyzz}	231	116.50
<γ>	157.457	79.31	**<γ>**	360	181.36
PNA <γ>[a]	1.246	6.27	PNA <γ>[a]	1.246	6.27

[a] The third-order nonlinear polarizabilities <γ> for *para*-nitroaniline (PNA) as calculated at the same PBE0/6-311G** level of theory in present investigation.

2 have centrosymmetric (with inversion symmetry) space group Triclinic, $P\bar{1}$ in its crystal packing, their second-order nonlinear polarizabilities are zero because according to the Kleinman approximation symmetry, centrosymmetry of crystals has no independent irreducible component of tensors, thus exhibiting no SHG effect. Nonetheless, these compounds are potentially dominated with third-order nonlinear polarizabilities (γ) regardless of their crystal space groups [31]. The third-order nonlinear polarizability is often considered as signature of rare observed two-photon absorption phenomenon. For third-order nonlinear polarizabilities, we have calculated their average third-order nonlinear polarizabilities **<γ>** and frequency dependent dynamic third-order polarizabilities related with dc-Kerr effect $\gamma(-\omega;\omega,0,0)$ [32] and EFISHG process $\gamma(-2\omega;\omega,\omega,0)$ [33]. The details about these processes at microscopic response level can be found from the given references [32]. The Table 3 shows the average static third-order nonlinear polarizabilities <γ> of comp.**1** and comp.**2** along with their individual tensors. It can be seen from Table 3 that the <γ> amplitudes of comp.**1** and comp.**2** are reasonably larger mounting to 79.31×10^{-36} and 181.36×10^{-36} esu at PBE0/6-311G** level of theory, respectively. In present investigation, just for comparative purpose, we have also calculated average static third-order nonlinear polarizabilities <γ> of *para*-nitroaniline (PNA) at same PBE0/6-311G** level of theory, which is usually considered a prototype/standard NLO molecule (see Table 3).

A comparison of average static third-order nonlinear polarizabilities <γ> shows that <γ> amplitudes of comp.**1** and comp.**2** are ~13 times and ~29 times larger than that of PNA at PBE0/6-311G** level of theory, which indicates a real time NLO application of our titled compounds. The <γ> amplitudes of comp.**2** is ~2 times larger as compared with that of comp.**1**, which is due to the enhanced electron donating effect of NR2 group in comp.**2**. Interestingly, a comparison of static third-order nonlinear polarizabilities <γ> with other similar types of compounds shows that the <γ> amplitudes of comp.**1** and comp.**2** have reasonably enhanced NLO response. For example, 3-acetyl-6-bromocoumarin [34] and 6-aminoquinoline (6AQ) [35] molecules showed 22.34×10^{-36} esu and 39.30×10^{-36} esu at CAM-B3LYP/6-311+G* and B3LYP/6-311++G** levels of theory, respectively. Among several complexes, the best studied beryllium–hydrocarbon complex has 139.30×10^{-36} esu at PBE0/6-311++G** level of theory [36], and conjugated TTF–quinones showed 4.13×10^{-36} and 4.66×10^{-36} esu at TDHF/6-311+G** level of theory [37]. In addition to static <γ> amplitudes, we have also calculated frequency dependent γ amplitudes for two different NLO processes [dc-Kerr effect $\gamma(-\omega;\omega,0,0)$ [32] and EFISHG process $\gamma(-2\omega;\omega,\omega,0)$ [33] at different wavelengths of incident laser. To check the effect of resonance enhancement, a wide range of frequency values ranging from fundamental frequency of 1907 nm to 544 nm are adopted as given in Table 4. A careful analysis of Table 4 shows that at 1907 nm the dynamic third-order nonlinear polarizabilities for $\gamma(-\omega;\omega,0,0)$ process are 85.04×10^{-36} and 202.61×10^{-36} esu for comp.**1** and comp.**2**, respectively. These values are larger than those of their static <γ> amplitudes and grad-

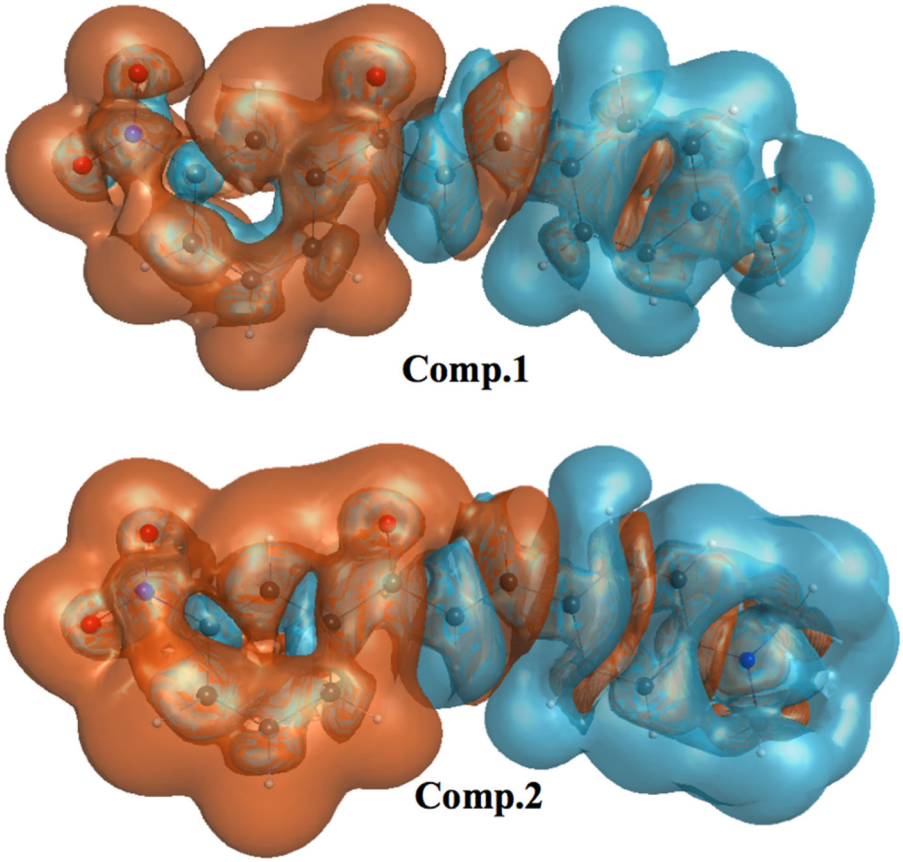

Fig. 5. γ density $\rho_{iii}^{(3)}(r)$ distributions for comp.**1** and comp.**2** where the golden and cyan meshes represent positive and negative γ densities with iso-surfaces of ±20.00 a. u., respectively.

Table 4
The calculated values of frequency dependent dynamic third-order polarizabilities related with dc-Kerr effect $\gamma(-\omega;\omega,0,0)$ [32] and EFISHG process $\gamma(-2\omega;\omega,\omega,0)$ [33] for comp.**1** and comp.**2** at PBE0/6-311G** level of theory.

Laser Type		Comp.**1**		Comp.**2**	
Energy (eV)	λ (nm)	$\gamma(-\omega;\omega,0,0)$ (10^{-36} esu)	$\gamma(-2\omega;\omega,\omega,0)$ (10^{-36} esu)	$\gamma(-\omega;\omega,0,0)$ (10^{-36} esu)	$\gamma(-2\omega;\omega,\omega,0)$ (10^{-36} esu)
0.650	1907	85.04	98.39	202.61	257.61
0.670	1851	85.41	99.80	204.04	263.84
0.689	1800	85.77	101.20	205.45	270.11
0.708	1751	86.16	102.74	206.97	277.11
0.775	1600	87.60	108.59	212.59	304.63
0.826	1500	88.83	113.91	217.49	331.07
0.885	1400	90.37	120.99	223.71	368.31
1.551	799	122.13	512.11	373.15	−11799
1.959	633	166.87	−399171	661.52	−295.97
2.280	544	236.49	585.35	1336.19	4001

ually increase with the decrease in wavelength of incident laser. There is no resonance enhancements observed for $\gamma(-\omega;\omega,0,0)$ process and the evaluation of frequency dependent γ amplitude is very significant at lower wavelengths as seen from Fig. 4. A somewhat similar trend with larger amplitudes for EFISHG process $\gamma(-2\omega;\omega,\omega,0)$ of frequency dependent dynamic third-order polarizabilities can be seen for both the compounds. At the most commonly used frequency of 1907 nm, the dynamic third-order nonlinear polarizabilities for $\gamma(-2\omega;\omega,\omega,0)$ process are 98.39×10^{-36} and 257.61 10^{-36} esu, which gradually increase to 585.35×10^{-36} and 4001×10^{-36} esu at 544 nm for comp.**1** and comp.**2**, respectively. There is resonance enhancement at 633 nm for comp.**1** and at 633 nm and 799 nm for comp.**2**, which is perhaps affected by resonance enhancement or re-absorption. Thus, care should be taken while considering frequency dependent third-order nonlinear polarizabilities of comp.**1** and comp.**2** below 900 nm for $\gamma(-2\omega;\omega,\omega,0)$ process. Usually, the compounds that have absorption between ω and 2ω show such kind of dispersion behaviors.

3.4. Origin of third-order nonlinear polarizability

To understand the origin of third-order NLO response in comp.**1** and comp.**2**, we have considered a simple approximation based on perturbative formula for static longitudinal γ_L value.

$$\gamma_L = 24\left[\frac{\mu_{ng}^2 \Delta\mu_{ng}^2}{\Delta E_{ng}^3} - \frac{\mu_{ng}^4}{\Delta E_{ng}^3}\right] \quad (7)$$

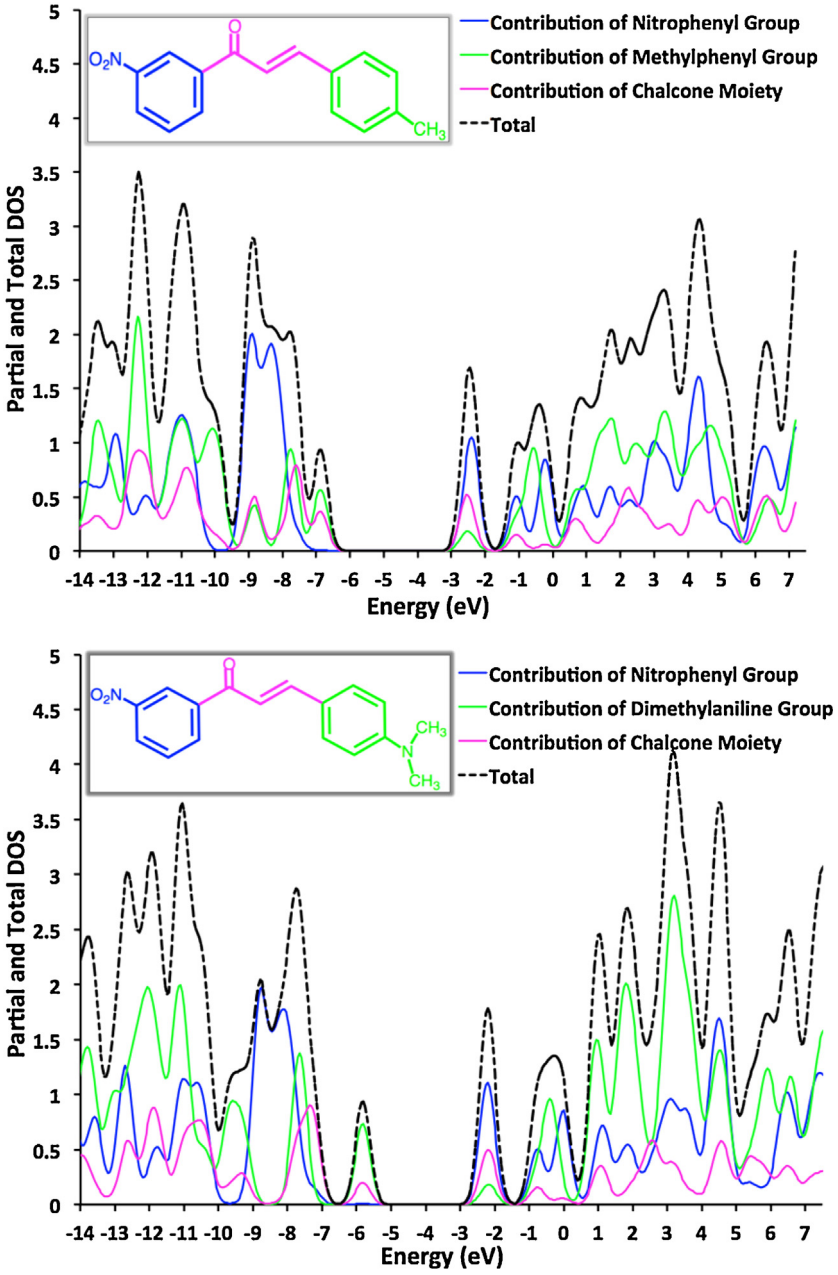

Fig. 6. Total densities of states (TDOS) and partial densities of states (PDOS) calculated at PBE0/6-311G* level of theory.

$$\gamma_L = 18\left[2\frac{\Delta\mu_{ng}^2 f_{ng}}{\Delta E_{ng}^3} - 3\frac{f_{ng}^2}{\Delta E_{ng}^5}\right] \quad (8)$$

where μ_{ng}, ΔE and $\Delta\mu$ are transition moment, transition energy and change in dipole moment related with transition from ground ($|g\rangle$) to crucial excited ($|n\rangle$) state. Similarly, f_{ng} is oscillatory strength, which is related to transition moment and transition energy as follow: $f_{ng} = \frac{2}{3}\Delta E_{ng}\mu_{ng}^2$. This so called two-level approximation is widely applied in theory and experiments to explain the changes in hyperpolarizabilities (β and γ) using spectroscopic parameters of several donor-acceptor types of molecules. For present investigation, the spectroscopic parameters are calculated with TD-DFT method including PBE0/6-311G** level of theory. From Eqs. (7) and (8), it can be seen that the transition energy term is in the denominator while transition moment, oscillatory strength and change in dipole moment terms are in nominator, which represents that any chemical system with lower transition energy and larger transition moment, oscillatory strength and change in dipole moments is expected to have larger γ amplitudes. The calculated values of f_o, ΔE and $\Delta\mu$ are collected in Table 5. For instance, comparing transition energies and oscillator strengths of comp.**1** and comp.**2**, it can be seen that the comp.**2** has lower transition energy of 3.18 eV with larger oscillator strength of 0.709 as compared to those of comp.**1**. Similarly, the change in dipole moment between ground to excited state for comp.**2** is larger having a value of ~11.35 a. u. as compared to that of ~2.76 a. u. for comp.**1**. It is important to mention that 10 low-lying excited states are calculated in present TD-DFT calculation and the first three are given in Table 5 where S_2 can be considered as crucial excited state in comp.**1** and comp.**2** due to their larger oscillator strengths and lower transition energies among all ten calculated excitations.

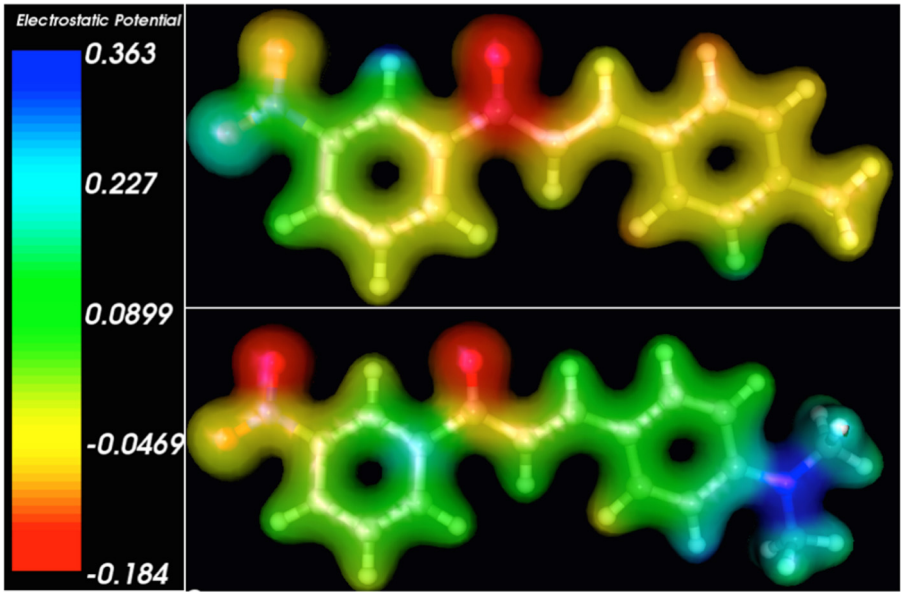

Fig. 7. Molecular electrostatic potential (MEP) diagram for comp.**1** and comp.**2** with isosurface value of 0.0400 a. u.

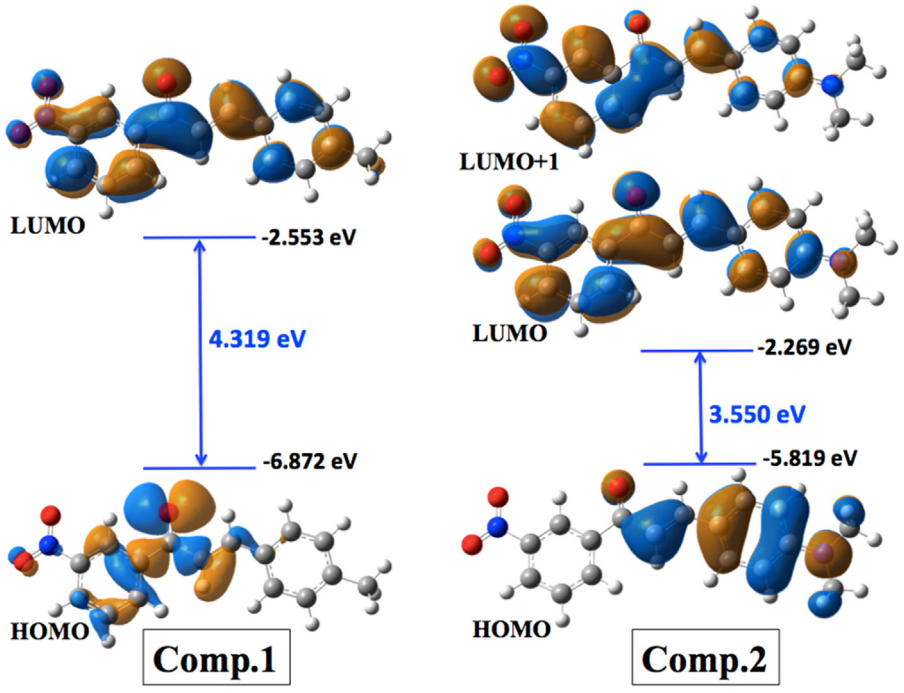

Fig. 8. The Frontier Molecular Orbitals along with their energy values and HOMO-LUMO energy gaps.

Table 5
The change in dipole moment between ground and excited states ($\Delta\mu$), oscillator strength (f_o), transition energies (ΔE), and% configuration interaction of crucial transitions at TD-PBE0/6311G** level of theory.

Sys.	$\Delta\mu$ (a. u.)[a]	Electronic Excitation	f_o	ΔE (eV)	Major Contribution	% C. I.
Comp.**1**	2.76	$S_0 \rightarrow S_1$	0.000	3.380	H−1 → L	67
		$S_0 \rightarrow S_2$	0.570	3.808	H → L	69
		$S_0 \rightarrow S_3$	0.013	3.986	H−4 → L	61
Comp.**2**	11.35	$S_0 \rightarrow S_1$	0.142	3.108	H → L	69
		$S_0 \rightarrow S_2$	0.709	3.282	H → L+1	69
		$S_0 \rightarrow S_3$	0.008	3.415	H−1 → L	51

[a] The $\Delta\mu$ is calculated at TD-PBE0/6311G** level of theory [b]S_1 excitation is not considered in comp.**1** because of its zero oscillator strength ($f_o \geq 0.000$).

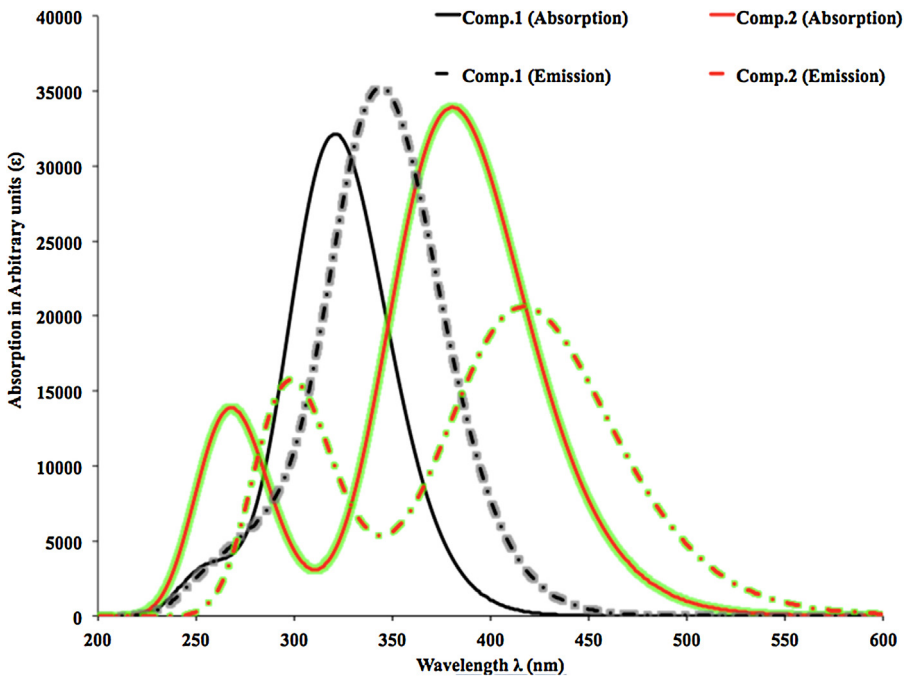

Fig. 9. The Absorption and emission spectra of comp.**1** and comp.**2** as calculated at TD- PBE0/6-311G** level of theory.

3.5. Hyperpolarizability γ density analysis

Using electron density derivatives, Nakano et al. [38,39] proposed a polarizability and hyperpolarizability analysis approach. This graphical analysis scheme use a direct plot of the electron density derivatives by presenting a new term of "(hyper)polarizability density". This quantity is useful for clarifying a spatial contribution of electrons to hyperpoalrizabilities and for illuminating the electron correlation effects on hyperpolarizabilities. The γ density $\rho_{iii}^{(3)}(\mathbf{r})$, describes the spatial electronic contributions to γ_{iii} value. This γ density is numerically calculated as the third-order derivative of electron density with respect to applied electric field:

$$\rho_{iii}^{(3)}(r) = \frac{\partial^3 \rho(r)}{\partial F_i \partial F_i \partial F_i}\Big|_{F=0} \tag{9}$$

Using this density, γ_{iii} is obtained by

$$\gamma_{iii} = -\frac{1}{3!}\int r_i \rho_{iii}^{(3)}(r)\, dr, \tag{10}$$

where r_i represents the i component of the position vector. It is noted that the positive and negative values of $\rho_{iii}^{(3)}(r)$ multiplied by F^3 correspond to the field induced increase and decrease in the electron density (in proportion to F^3), which induce the third-order dipole moment (third-order polarization) in the direction from positive to negative densities. From Fig. 5, it can be seen that the contributions taken from a pair of positive and negative γ densities provide a description of local contributions of electrons, i.e., field-induced third-order dipole moment, to the total γ. Similarly, the primary positive and negative γ densities in comp.**1** and comp.**2** show clear distributions with larger amplitudes towards the left and right edges containing acceptor and donor groups, respectively. Furthermore, the γ density distribution plots show that π-electrons provide the major (positive) contributions to the γ values especially in comp.**2** with larger amplitudes positive and negative γ densities (see Fig. 5).

3.6. Density of states

Using AOMix wave function analysis program [40], the total density of states (TDOS) and partial density of states (PDOS) are calculated for both the molecules. The TDOS and PDOS are calculated to understand the role of individual molecular fragments into the bonding and electro-optical properties of studied systems. We generate the TDOS and PDOS plots by dividing the molecule into three fragments i.e. donor, acceptor and chalcone fragments (see Fig. 6). The TDOS and PDOS plots shows population analysis per orbital and illustrates the view of the modest makeup for the molecular orbitals in a certain energy range while PDOS plot shows percentage contribution of each fragment to each molecular orbital in the final molecule.

From Fig. 6, it can be seen that valence orbitals contain more contribution from donor fragments where the contribution of Ph-$N(CH_3)^2$ is also relatively more as compared to that of Ph-CH_3 group. According to DOS of comp.1 and comp.2, it can be seen that there is significant change in electronic structure when methyl group is replaced with dimethylamine group, where the later is more efficient donor group in above push-pull configuration. The HOMO-LUMO energy gap (ΔE_{HL}) has been also reduced from 4.320 eV of comp.**1** to 3.550 eV in comp.**2**. The decrease in 0.77 eV in ΔE_{HL} energy is corresponds to stronger push-pull configuration in comp.**2**. The contribution of Ph-$N(CH_3)^2$ fragment to the TDOS of comp.**2** is not only significant in HOMO orbital energy level but also presents substantial contribution to the TDOS in energy range from 0.5 eV to 4 eV in conduction band.

3.7. Molecular electrostatic potential

We have also calculated the molecular electrostatic potential (MEP) plots for comp.**1** and comp.**2** using the molecular charge density within following standard approach:

$$V(r) = \sum_{\alpha}\frac{Z_\alpha}{r - R_\alpha} - \int \frac{\rho(r')}{r - r'}dr', \tag{11}$$

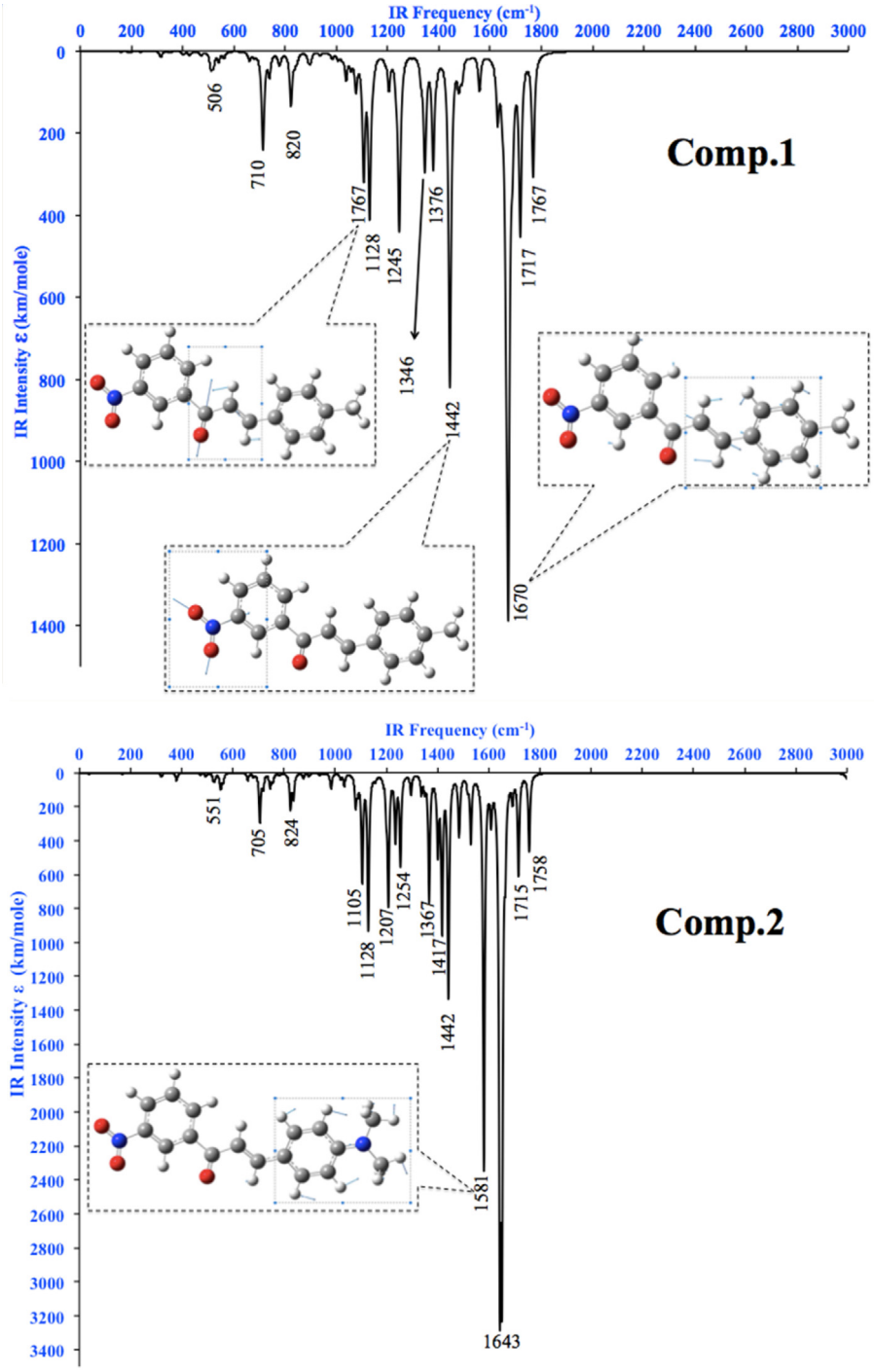

Fig. 10. The IR spectra of comp.**1** and comp.**2** at PBE0/6-311G** level of theory while inside Figures show the displacement vectors for different vibrational moods.

where Z_α represents a charge of the α-th nucleus at position R_α. These MEPs provide several comprehensive intuitives about the distribution of electrostatic charges on the optimized ground state geometries of comp.**1** and comp.**2** as given in Fig. 7. For instance, a maximum negative region is preferred site for electrophilic attack is indicated as red surface while the maximum positive region that is preferred site for nucleophilic attack indicated as blue color on MEP surface. A careful analysis of Fig. 7 illustrates that the distribution of molecular charge density is more uniform in comp.**1** leading to less polarized ground state. On the other hand, the MEP of comp.**2** depicts a more charge separated ground state where negative charge is seen around carbonyl oxygen atoms and positive charge density on nitrogen atom of Ph-$N(CH_3)^2$ group. Interestingly, the MEP plots are also inline with above reported electronic dipole moments. For instance, the dipole moments are 3.25 and 4.63 a. u. and having an angle of 45° with central z-axis for comp.**1** and comp.**2**, respectively (see Fig. 2). The larger dipole moment and its direction for comp.2 is easily comprehensible through the prism of MEP of comp.2 with a clear negative and positive charge separation between carbonyl and $N(CH_3)^2$ group, respectively.

3.8. Frontier molecular orbitals (FMO)

The FMOs play a very important role to determine the reactivity of a chemical compound as well as it is also crucial implications of an organic material in organic semiconductors. The FMOs for

comp.**1** and comp.**2** are illustrated in Fig. 8 along with their energy levels and HOMO-LUMO energy gaps (E_g). A comparison of orbital energy gaps represents that comp.**2** has lower E_g value of 3.550 eV as compared to 4.319 eV of comp.**1**, which results in a lower energy electron transition. From Fig. 8, it can be seen that the nature of transition is very different in comp.**1** and comp.**2**. In comp.**1**, during transition the electron density has been transfer from HOMO (mainly localized on carbonyl and nitrophenyl ring) to LUMO (delocalized over the whole π-skeleton) of comp.**1**, which prominently a nonbonding *n* to π* type of transition with lower oscillator strength. On the other hand, the electronic transition in comp.**2** clearly posses the intramolecular charge transfer characteristic resulting from the transfer of electronic cloud from NR_2 donor moiety to the nitrophenyl acceptor group.

3.9. Absorption and emission spectra

The TD-DFT calculations have been used to calculate the absorption and emission Spectra of comp.**1** and comp.**2** as given in Fig. 9. The absorption spectrum (solid lines) of comp.**1** is significantly different than that of comp.**2**. For instance, the maximum absorption of comp.**1** is calculated at 325 nm with a slight shoulder band at about 255 nm while on the other hand, the absorption spectrum of comp.**2** shows two distinct absorption peaks at 377 and 267 nm. A red shift of 52 nm is found comparing absorption spectrum of comp.**1** and comp.**2**, which is attributed to the stronger push-pull configuration in comp.**2** due to stronger NR_2 donating group. The nature of transition in comp.**1** is nonbonding *n* to π^* while in comp.**2** the electron density transfer process shows a π to π* transition as it is explained in frontier molecular orbitals (FMO) section. Similarly, the wavelengths of emission have also shown a maximum emission peaks at 343 and 417 nm for comp.**1** and comp.**2**, respectively. The comparison of absorption and emission spectra indicates the stock shifts of 18 nm and 40 nm for comp.**1** and comp.**2**, respectively.

3.10. IR vibrational spectra

To the best of our knowledge, there is still no report about the IR spectra of comp.**1** and comp.**2**. The IR spectrum is based on the fact that interatomic bonds in organic compounds absorb the electromagnetic radiations in the range of ~4000 cm^{-1}–400 cm^{-1}. These frequencies of absorbed radiations are correlated with bonds of newly studied compounds. In present investigation, the IR spectra are calculated at PBE0/6-311G** level of theory. The frequencies are not further subjected to any scaling factor because there are no available experimental IR spectra for these compounds. The comp.**1** and comp.**2** consist of 33 atoms and 38 atoms, which show 93 and 108 fundamental vibrational moods in these compounds, respectively. All the vibrations from frequency 0 to 3000 cm^{-1} are included in both IR spectra as shown in Fig. 10. Different absorption intensities for characteristic vibrational IR frequencies can be seen for comp.**1** and comp.**2**. For instance, IR spectrum of comp.**1** shows highest intensity peak at 1670 cm^{-1} related with symmetric stretching vibration of C=C and bending vibration of C—H bonds in 4-methylphenyl moiety as shown their vibrational displacements in inside of Fig. 10. Similarly, the peaks at 1442 cm^{-1} and 1767 cm^{-1} show stretching vibrations of NO2 and C=O groups, respectively. Comparing IR spectrum of comp.**2** with IR spectrum of comp.**1** shows that there is overall a slight red shift in wavenumbers along with appearance of a new peak at 1581 cm^{-1} related with H-atoms bending vibrations in *N*,*N*-dimethylaniline group. In addition to change in frequency value, there is also significant increase in IR absorption intensity of comp.**2**. For example, the highest intensity peak at 1670 cm^{-1} has intensity of 1400 km/mole, which increased to 3300 km/mole at 1643 cm^{-1} in comp.**2**, which is perhaps to the stronger donor-acceptor configuration of comp.**2**. Thus the present IR spectra evaluation would be helpful to confirm the compounds where sophisticated techniques single crystal analyses are not available.

4. Conclusions

Thus the present investigation for the first time put into limelight the importance of above titled chalcone comp.**1** and comp.**2**. It is found that the tuning of only donor end (replacing CH_3 with *N*-$(CH_3)_2$) can significantly enhance the third-order NLO response without affecting the acceptor end in donor-π-conjugation-acceptor configuration. Interestingly, substitution of *N*,*N*-dimethylaniline of comp.**2** results a remarkable increase in its <γ> amplitude, which is ~2 times larger as compared with that of comp.**1** owing to the stronger donor-acceptor configuration of comp.**2**. Additionally, the origin of the enhancement of <γ> amplitude in comp.**2** has been traced using TD-DFT calculations within the framework of perturbative formula for static longitudinal γ_L values. For instance, it has been found that the lower transition energy, larger oscillator strength and more change in dipole moment from ground to excited state play a crucial role to boost the <γ> amplitude in comp.**2**. Interestingly, a comparison of average static third-order nonlinear polarizabilities <γ> shows that <γ> amplitudes of comp.**1** and comp.**2** are ~13 times and ~29 times larger than that of *para*-nitroaniline (PNA) at PBE0/6-311G** level of theory, which indicates a real time NLO application of our titled compounds. Additionally, for the first time, the DOS, MEP, FMOs, absorption, emission and IR spectra of the above compounds are also established. It is expected the present investigation will not only put these compounds under the spotlight of recent scientific interest but also establish a structure-NLO property relation for their hi-tech laser and NLO applications.

Acknowledgements

Authors would like to acknowledge the support of the International Coordination Unit, King Khalid University (KKU) for this research through a Grant (RCAMS/KKU/001-16) under the Research Center for Advanced Materials Science (RCAMS) at KKU, Kingdom of Saudi Arabia. The authors also acknowledge the sharing of computational resources from Northeast Normal University, China for present work.

Appendix A. Supplementary data

Supplementary data associated with this article can be found, in the online version, at http://dx.doi.org/10.1016/j.jmgm.2016.12.009.

References

[1] M.G. Papadopoulos, A.J. Sadlej, J. Leszczynski, Non-linear Optical Properties of Matter, Springer, 2006.
[2] S. Muhammad, H.-L. Xu, R.-L. Zhong, Z.-M. Su, A.G. Al-Sehemi, A. Irfan, Quantum chemical design of nonlinear optical materials by sp 2-hybridized carbon nanomaterials: issues and opportunities, J. Mater. Chem. C 1 (2013) 5439–5449.
[3] R.W. Munn, C.N. Ironside, Principles and Applications of Nonlinear Optical Materials, Springer, 1993.
[4] T. Verbiest, S. Houbrechts, M. Kauranen, K. Clays, A. Persoons, Second-order nonlinear optical materials: recent advances in chromophore design, J. Mater. Chem. 7 (1997) 2175–2189.
[5] S. Muhammad, M.R.S.A. Janjua, Z. Su, Investigation of dibenzoboroles having π-electrons: toward a new type of two-dimensional NLO molecular switch? J. Phys. Chem. C 113 (2009) 12551–12557.
[6] P. Judeinstein, C. Sanchez, Hybrid organic–inorganic materials: a land of multidisciplinarity, J. Mater. Chem. 6 (1996) 511–525.
[7] S. Muhammad, H. Xu, Z. Su, K. Fukuda, R. Kishi, Y. Shigeta, et al., A new type of organic–inorganic hybrid NLO-phore with large off-diagonal first

hyperpolarizability tensors: a two-dimensional approach, Dalton Trans. 42 (2013) 15053–15062.
[8] S. Muhammad, T. Minami, H. Fukui, K. Yoneda, R. Kishi, Y. Shigeta, et al., Halide ion complexes of decaborane (B10H14) and their derivatives: noncovalent charge transfer effect on second-Order nonlinear optical properties, J. Phys. Chem. A 116 (2012) 1417–1424.
[9] F. Terenziani, C. Katan, E. Badaeva, S. Tretiak, M. Blanchard-Desce, Enhanced two-photon absorption of organic chromophores: theoretical and experimental assessments, Adv. Mater. 20 (2008) 4641–4678.
[10] S. Alen, D. Sajan, L. Joseph, K. Chaitanya, V. Shettigar, V.B. Jothy, Synthesis, growth, vibrational spectral investigations and structure–property relationship of an organic NLO crystal: 3,4-dimethoxy chalcone, Chem. Phys. Lett. 636 (2015) 208–215.
[11] A.P. Menezes, A. Jayarama, S.W. Ng, Crucial role of molecular planarity on the second order nonlinear optical property of pyridine based chalcone single crystals, J. Mol. Struct. 1088 (2015) 85–94.
[12] A.A. Prasad, K. Muthu, V. Meenatchi, M. Rajasekar, R. Agilandeshwari, K. Meena, et al., Optical, vibrational, NBO, first-order molecular hyperpolarizability and Hirshfeld surface analysis of a nonlinear optical chalcone, Spectrochim. Acta Part A 140 (2015) 311–327.
[13] S.R. Prabhu, A. Jayarama, V. Upadhyaya, K.S. Bhat, S.W. Ng, Structure and characterization of a novel chalcone crystal having nitro as an acceptor group, Mol. Cryst. Liquid Cryst. 607 (2015) 200–214.
[14] P.S. Patil, P.A. Kumar, S.V. Rao, G. Bhagavannarayana, Growth and characterization of a new organic nonlinear optical crystal: 1-(3-nitrophenyl)-5-phenylpenta-2, 4-dien-1-one, Opt. Laser Technol. 71 (2015) 108–113.
[15] B.C. Hemaraju, A.P. Gnana Prakash, Growth, optical, thermal and dielectric studies of new organic nonlinear optical crystal (R)-2-cyano-N-(1-phenylethyl)acetamide, Optik—Int. J. Light Electron Opt. 126 (2015) 3049–3052.
[16] S. Raghavendra, C.S. Dileep, S.M. Dharmaprakash, Nonlinear absorption, and optical limiting properties of a new organic crystal 3-(3-fluorophenyl)-1-[4-(methylsulfanyl) phenyl] prop-2-en-1-one, Mol. Cryst. Liquid Cryst. 609 (2015) 192–204.
[17] K. Thanigaimani, S. Arshad, N.C. Khalib, I.A. Razak, C. Arunagiri, A. Subashini, et al., A new chalcone structure of (E)-1-(4-bromophenyl)-3-(napthalen-2-yl) prop-2-en-1-one: synthesis, structural characterizations, quantum chemical investigations and biological evaluations, Spectrochim. Acta Part A 149 (2015) 90–102.
[18] S. Muhammad, H. Xu, Y. Liao, Y. Kan, Z. Su, Quantum mechanical design and structure of the Li@ B10H14 basket with a remarkably enhanced electro-optical response, J. Am. Chem. Soc. 131 (2009) 11833–11840.
[19] S. Muhammad, H. Xu, M.R.S.A. Janjua, Z. Su, M. Nadeem, Quantum chemical study of benzimidazole derivatives to tune the second-order nonlinear optical molecular switching by proton abstraction, PCCP 12 (2010) 4791–4799.
[20] S. Muhammad, A. Irfan, M. Shkir, A.R. Chaudhry, A. Kalam, S. AlFaify, et al., How does hybrid bridging core modification enhance the nonlinear optical properties in donor-π-acceptor configuration? A case study of dinitrophenol derivatives, J. Comput. Chem. 36 (2015) 118–128.
[21] S. Muhammad, A.G. Al-Sehemi, A. Irfan, A.R. Chaudhry, Tuning the push-pull configuration for efficient second-order nonlinear optical properties in some chalcone derivatives, J. Mol. Graphics Modell. 68 (2016) 95–105.
[22] S. Muhammad, A.G. Al-Sehemi, A. Irfan, A.R. Chaudhry, H. Gharni, S. AlFaify, et al., The impact of position and number of methoxy group (s) to tune the nonlinear optical properties of chalcone derivatives: a dual substitution strategy, J. Mol. Model. 22 (2016) 1–9.
[23] J.P. Jasinski, R.J. Butcher, B. Narayana, K. Lakshmana, H.S. Yathirajan, (2E)-3-(4-Methylphenyl)-1-(3-nitrophenyl) prop-2-en-1-one, Acta Crystallogr. Sect. Sect. E: Struct. Rep. Online 64 (2008) o1–o2.
[24] M.M. Rosli, P.S. Patil, H.K. Fun, I.A. Razak, S.M. Dharmaprakash, (2E)-3-[4-(Dimethylamino) phenyl]-1-(3-nitrophenyl) prop-2-en-1-one, Acta Crystallogr. Sect. Sect. E: Struct. Rep. Online 63 (2007) o2692–o.
[25] M.J. Frisch, G.W. Trucks, H.B. Schlegel, G.E. Scuseria, M.A. Robb, J.R. Cheeseman, et al., Gaussian 09, Gaussian, Inc, Wallingford, CT, 2009, There is no corresponding record for this reference.
[26] D. Jacquemin, E.A. Perpete, I. Ciofini, C. Adamo, Accurate simulation of optical properties in dyes, Acc. Chem. Res. 42 (2008) 326–334.
[27] S. Muhammad, Second-order nonlinear optical properties of dithienophenazine and TTF derivatives: a butterfly effect of dimalononitrile substitutions, J. Mol. Graph. Modell. 59 (2015) 14–20.
[28] H.A. Kurtz, J.J.P. Stewart, K.M. Dieter, Calculation of the nonlinear optical properties of molecules, J. Comput. Chem. 11 (1990) 82–87.
[29] M. Shkir, S. AlFaify, H. Abbas, S. Muhammad, First principal studies of spectroscopic (IR and Raman, UV–visible), molecular structure, linear and nonlinear optical properties of l-arginine p-nitrobenzoate monohydrate (LANB): a new non-centrosymmetric material, Spectrochim. Acta Part A 147 (2015) 84–92.
[30] C. Dehu, F. Meyers, J.L. Bredas, Donor-acceptor diphenylacetylenes: geometric structure, electronic structure, and second-order nonlinear optical properties, J. Am. Chem. Soc. 115 (1993) 6198–6206.
[31] J. Zyss, J.L. Oudar, Relations between microscopic and macroscopic lowest-order optical nonlinearities of molecular crystals with one-or two-dimensional units, Phys. Rev. A 26 (1982) 2028.
[32] E. Cottancin, M. Broyer, J. Lermé, M. Pellarin, Handbook of Nanophysics: Nanoelectronics and Nanophotonics. Chapter 27: Nonlinear Optics with Clusters, KD Sattler, Taylor and Francis group, 2010, pp. 1–2.
[33] K. Rottwitt, P. Tidemand-Lichtenberg, Nonlinear Optics: Principles and Applications, CRC Press, 2014.
[34] A.N. Castro, L.R. Almeida, M.M. Anjos, G.R. Oliveira, H.B. Napolitano, C. Valverde, et al., Theoretical study on the third-order nonlinear optical properties and structural characterization of 3-acetyl-6-bromocoumarin, Chem. Phys. Lett. 653 (2016) 122–130.
[35] P.S.P. Silva, H. El Ouazzani, M. Pranaitis, M.R. Silva, C.T. Arranja, A.J.F.N. Sobral, et al., Experimental and theoretical studies of the second-and third-order NLO properties of a semi-organic compound: 6-aminoquinolinium iodide monohydrate, Chem. Phys. 428 (2014) 67–74.
[36] K. Hatua, P.K. Nandi, Theoretical study of electronic structure and third-order optical properties of beryllium-hydrocarbon complexes, Comp. Theor. Chem. 996 (2012) 82–90.
[37] A. Karakas, A. Migalska-Zalas, Y. El Kouari, A. Gozutok, M. Karakaya, S. Touhtouh, Quantum chemical calculations and experimental studies of third-order nonlinear optical properties of conjugated TTF–quinones, Opt. Mater. 36 (2013) 22–26.
[38] M. Nakano, K. Yamaguchi, T. Fueno, Coupled-hartree—fock calculations of the third-order hyperpolarizabilities of substituted polydiacetylenes, Chem. Phys. Lett. 185 (1991) 550–554.
[39] S. Muhammad, K. Fukuda, T. Minami, R. Kishi, Y. Shigeta, M. Nakano, Interplay between the diradical character and third-order nonlinear optical properties in fullerene systems, Chem.—Eur. J. 19 (2013) 1677–1685.
[40] S.I. Gorelsky, A.B.P. Lever, Electronic structure and spectra of ruthenium diimine complexes by density functional theory and INDO/S. Comparison of the two methods, J. Organomet. Chem. 635 (2001) 187–196.